Dusty disks around young brown dwarfs

Lucía Adame (IA-UNAM), Paola D'Alessio (CRyA-UNAM)
and Nuria Calvet (UMich)

Abstract

We modify the computational codes developed by D'Alessio and colaborators to obtain the IRAC synthetic colors for young brown dwarfs with disks in Taurus. A set of models, ranging several mass accretion rates, substellar effective temperature, and alpha-viscosity parameter, are constructed; with that, and using previously published IRAC data, we study the innermost region of the circunsubstellar accretion disks in the Taurus region. The median SED of Taurus for stellar/substellar objects with spectral types between M6 and M9 is obtained.

With the advent of the Spitzer Space Telescope (SST, Werner et al., 2004), a plethora of dusty disks around young substellar objects was discovered. The Taurus-Auriga molecular cloud is a well-known and nearby star-forming region, and because its young age, a place to spy brown dwarfs still in their *T Tauri phase*. The study of accretion disks around substellar objets can help us to differentiate the mechanism of brown dwarf formation, but mainly, to understand the differences, if any, between them and the disks around T Tauri stars.

1 Observed median SED

We constructed the observed median SED for young brown dwarfs in Taurus compiling published photometry from the Point Source Catalog of the Two Micron All Sky Survey (2MASS J, H, and K_s bands, Skrutskie et al., 2006), the IRAC (Fazio et al., 2004) and MIPS (Rieke et al., 2004) instruments aboard the SST (Werner et al., 2004), and 1.3 mm-fluxes. 2MASS and IRAC photometry were obtained mostyl from Luhman (2004); Luhman et al. (2006), IRAC and MIPS-24μm flux from Guieu et al. (2007) and millimetric flux from Scholz et al. (2006). We select objects from these surveys with spectral type later or equal than M6, which at the age of the Taurus region, have masses near or below the hydrogen-burning mass limit (e.g., Luhman et al., 2006). We eliminated brown dwarfs with IRAC colors indicative of photospheric colors, i.e., brown dwarfs without a *normal, non-truncated* dusty disk, $[3.6]-[4.5] \lesssim 0.15$ and $[5.8]-[8] \lesssim 0.3$ (Hartmann et al., 2005; Luhman et al., 2006), and the brown dwarf 2MASS J04381486 + 2611399 due to its anomalous near-IR colours (this object has a nearly edge-on accretion disk, Luhman, 2004; Luhman et al., 2007); also, objects with binary companions were discarded. Table 1 lists the substellar

objects used to construct the observed median SED, adopting in this case the luminosity estimate from the magnitude K_s, L_K (if L_J was not reported; in any case, differences between these luminosity values are $\lesssim 35\%$; also, it has to be tested a posteriory if the magnitude K_s is not contaminated by the emission from the inner disk). Thirteen objects raging from spectral type M6 down to M9 comprises our subset of brown dwarfs in Taurus, out of 52 known substellar objects with spectral type later or equal than M6. Several of the non-selected brown dwarfs are known to be substellar objects because its JHK_s photometry, and because their lack of published IRAC photometry cannot be included in our subset until evidence of excess emission is provided.

Table 1: Brown dwarfs selected to construct the substellar observed median SED

2MASS ID	Name	Spectral Type	$L_*[10^{-2}L_\odot]$
J0419012+280248	KPNO-Tau 12	M9	0.09
J04230607+2801194		M6	3.40
J04242090+2630511		M6.5	1.10
J04262939+2624138	KPNO-Tau-3	M6	2.00
J04290068+2755033		M8.25	0.70
J04300724+2608207	KPNO-Tau 6	M8.5	0.30
J04305718+2556394	KPNO-Tau 7	M8.25	0.40
J04382134+2609137	GM Tau	M6.5	4.70
J04390396+2544264	CFHT-6	M7.25	2.00
J04394748+2601408	CFHT-Tau-4	M7	5.40
J04400067+2358211		M6	3.00
J04414825+2534305		M7.75	0.92
J04442713+2512164	IRAS04414+2506	M7.25	2.80

The median SED for JHK_s and IRAC bands is constructed once the fluxes are normalized at 1.66μm (assuming correctly that the main disk's heating agent is the stellar/substellar radiation, D'Alessio et al., 1999; Adame , 2009). Flux at 24μm is available only for 6 objects (plus one upper limit) of our sample, and the mm-flux was measured for 4 of the 13 objects; 3 of these 13 were undetected. Due to this incompleteness, median SED models obtained for $\lambda \gtrsim 24\mu$m solely indicates a trend, but they are worth to be constructed. Table 2 shows median fluxes and quartiles for the selected brown dwarfs. The construction of the median at $\lambda = 24\mu$m and 1.3mm considers only detections; for comparison purposes with the models, we constructed the median for 70μm, based on upper-limit fluxes reported by Guieu et al. (2007). The observed median SED is shown in Figure 1.

From Figure 1, it is tempting to conclude that disks around substellar objects are scaled versions of their more massive counterparts; this might be real when considering the innermost region only. But to which extent this is true for all radii is not yet conclusive; the synthetic best-fit models for the observed median SED, constructed as described in (D'Alessio et al., 2005, 2006; Adame , 2009) (mass acretion rate of $\log \dot{M} = -11, -10$, $\log \alpha = -5, -4$, dust-depletion parameter $\epsilon = 0.001 - 0.01$, inclination angle $i = 50\,\mathrm{deg}$, outer disk radii $R_d = 10 - 50$AU, dusty inner disk truncated at $T_w = 1400$K), show that circumsubstellar

Table 2: Median SED and quartiles for young brown dwarfs with disks

Band	Lower Quartile	Median	Upper Quartile
J	24.3700	26.2700	26.7300
H	23.8700	23.8700	23.8700
K_s	17.4800	18.4100	19.4600
3.6	7.6720	8.7200	10.1800
4.5	5.4140	5.8080	8.2060
5.8	3.8590	4.3160	5.8290
8	3.0570	3.4180	4.3580
24	1.3020	1.6660	2.5780
70	...	3.0450	7.1720
1.3mm	0.0037	0.0062	0.0081

accretion disks need to have very low α values (being α the turbulent viscosity parameter in the context of α-disks), $\alpha \lesssim 10^{-4}$ to fit fluxes at $\lambda \gtrsim 24\mu$m (see, for example, the discussion in Luhman et al., 2007), while circumstellar accretion diks requires $\alpha \approx 10^{-2}$ (e.g. D'Alessio et al., 1999, and references therein). Further observations are required in this wavelength range to refine the observed median SED and thus to obtain reliable conclusions on the nature of the circumsubstellar accretion disk.

Back to the innermost region, it is crucial to have a dependable estimate of the substellar photosphere at IRAC wavelengths. Panel (a) of Figure 1 shows the Allard photosphere for a brown dwarf with $T_{eff} = 2800$K and the observed SED for a brown dwarf with spectral type M7.25 (see Luhman et al., 2007, for details); while the first implies [3.6] excess (and thus, the presence of warm dust at $T \approx 1400$K in the disk), the observed photospheric flux at [3.6] can explain the observed median. The immediate conclusion is twofold: while the apparent no-excess at [3.6] can be explained invoking an inner hole (with $T_w < 1400$K) larger than the *normal* truncation radius, a depleted wall with scaleheights $\lesssim 1H_p$ (H_p is the gas scaleheight at $T = 1400$K) can explain the observed excess at [4.5], [5.8] and [8].

2 Synthetic IRAC colors

For our median brown dwarf ($M_* = 0.05M_\odot$, $L_* = 0.02L_\odot$, $T_{eff} = 2838$K), we construct models for dusty accretion disks as described in D'Alessio et al. (2005, 2006); Adame (2009), varying the α-viscosity parameter ($\log\alpha = -5, -4$), the mass accretion rate ($\log\dot{M} = -11, -10$), the temperature of the vertical wall (and thus the inner disk radius; $T_w = 700, 1000, 1400$K) and its height ($H_{wall} = 0.1, 0.5, 1, 3, 5H_p$), the dust depletion parameter ($\epsilon = 0.0001, 0.001, 0.01, 1$), and the outer disk radius ($R_d = 10, 50, 100$AU). For all the cases, synthetic IRAC colors, varying the inclination angle of the disk ($\mu = 0.25, 0.5, 0.87, 0.985$), were computed using the photosphere of the M7.25 dwarf of Luhman et al. (2007); resulting color-color diagrams are shown in Figures 2 and 3. From these, it is evident that there exists a degeneration in the space parameter; to break this degeneration longer wavelength observation, for example, is needed. In any case, models with inclination angles smaller or equal

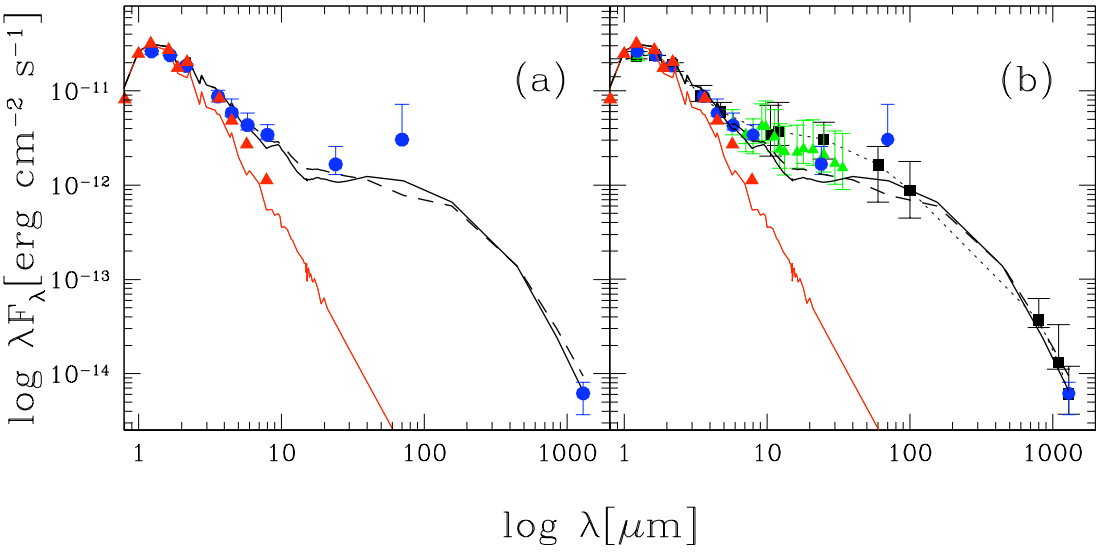

Figure 1: Observed median SED for young brown dwarfs with disks in Taurus. Panel (a): Observed median SED (*blue filled circles*) constructed for the sample listed in Table 1; the two disk+wall best-fit models are shown for comparison (*continuous and long-dash lines;*see text for explanation). The Allard photosphere (Allard et al., 2001) for a dwarf with T_{eff} = 2800K and $L_* = 0.02 L_\odot$ (*red line*) The photosphere from a *typical* M7.25 (T_{eff} = 2838K, $L_* = 0.02 L_\odot$) dwarf, from Luhman et al. (2007) is shown for comparison (*red triangles*). Panel (b): Comparison with the observed median SEDs reported by D'Alessio et al. (1999) (*filled black squares and dotted line*) and Furlan et al. (2006) (*filled green triangles*), scaled at 1.66μm

than 60 deg (almost pole-on) are favored over nearly edge-on inclinations. Also, models with $\alpha \lesssim 10^{-4}$, relatively large wall heights, larger mass accretion rate, smaller outer disk radius, seems to explain some observed colors. For 5 brown dwarfs, it seems that the temperature of the wall is smaller than 1400K, as the region where non-truncated disks are located lies between well defined colors. Figure 3 should not be used blindly, because the [8] band is contaminated by the silicate emission (D'Alessio et al., 2006); but nevertheless it is a useful diagram when discriminating brown dwarfs with or without disks.

Bibliography

Adame, L. PhD thesis, Universidad Nacional Autónoma de México

Allard, F., Hauschildt, P. H., Alexander, D. R., Tamanai, A., & Schweitzer, A. 2001, apj, 556, 357

D'Alessio, P., Calvet, N., Hartmann, L., Lizano, S., & Cantó, J. 1999, ApJ, 527, 893

D'Alessio, P., et al. 2005, ApJ, 621, 461

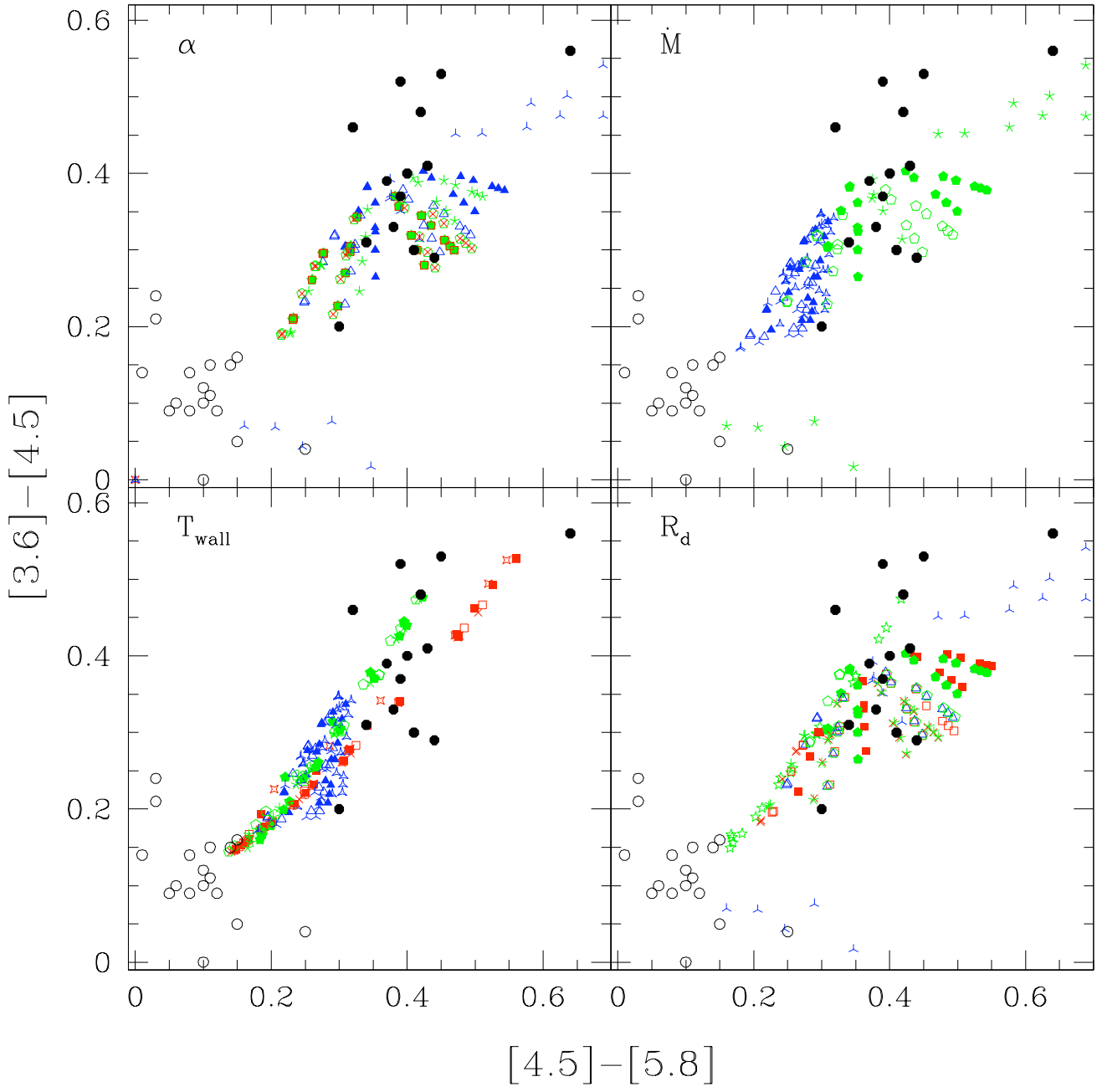

Figure 2: Synthetic color-color plot for young brown dwarfs in Taurus, eliminating the [8]-band;. Each panel specifies which parameter is varied. From left-upper panel and clockwise, (α): models for $\log \dot{M} = -10$, varying α ($\alpha = 10^{-2}$, *green*; 10^{-4}, *red*and 10^{-5}, *blue*). ($\dot{M}$): models for $\alpha = 10^{-5}$, varying $\dot{M}$ ($\log \dot{M} = -11$, *blue*; -10, *green*). (R_d): models for $\log \dot{M} = -10$, $\alpha = 10^{-5}$, varying the outer disk radius ($R_d = 10$AU, *red*; 50AU, *blue* and 100AU, *green*). (T_{wall}): models for $\log \dot{M} = -11$, $\alpha = 10^{-5}$, varying the inner disk radius ($T_{wall} = 700$K, *red*; 1000K, *green* and 1400K, *blue*). *Filled black circles*: observed colors of our brown dwarf set; *empty black circles*: observed colors of the *diskless* set of brown dwarfs. For the synthetic models, the form of the symbol represents the dust depletion parameter: *skeletal, or the center connected to the vertices*, $\epsilon = 0.001$; *empty*, $\epsilon = 0.01$;*filled*, $\epsilon = 0.1$ and *starred*, $\epsilon = 1$. Each symbol denotes the same model as the symbol color. The $[4.5] - [5.8]$ color is larger when increasing the inclination angle, while the $[3.6] - [4.5]$ color increases when decreasing the height of the wall

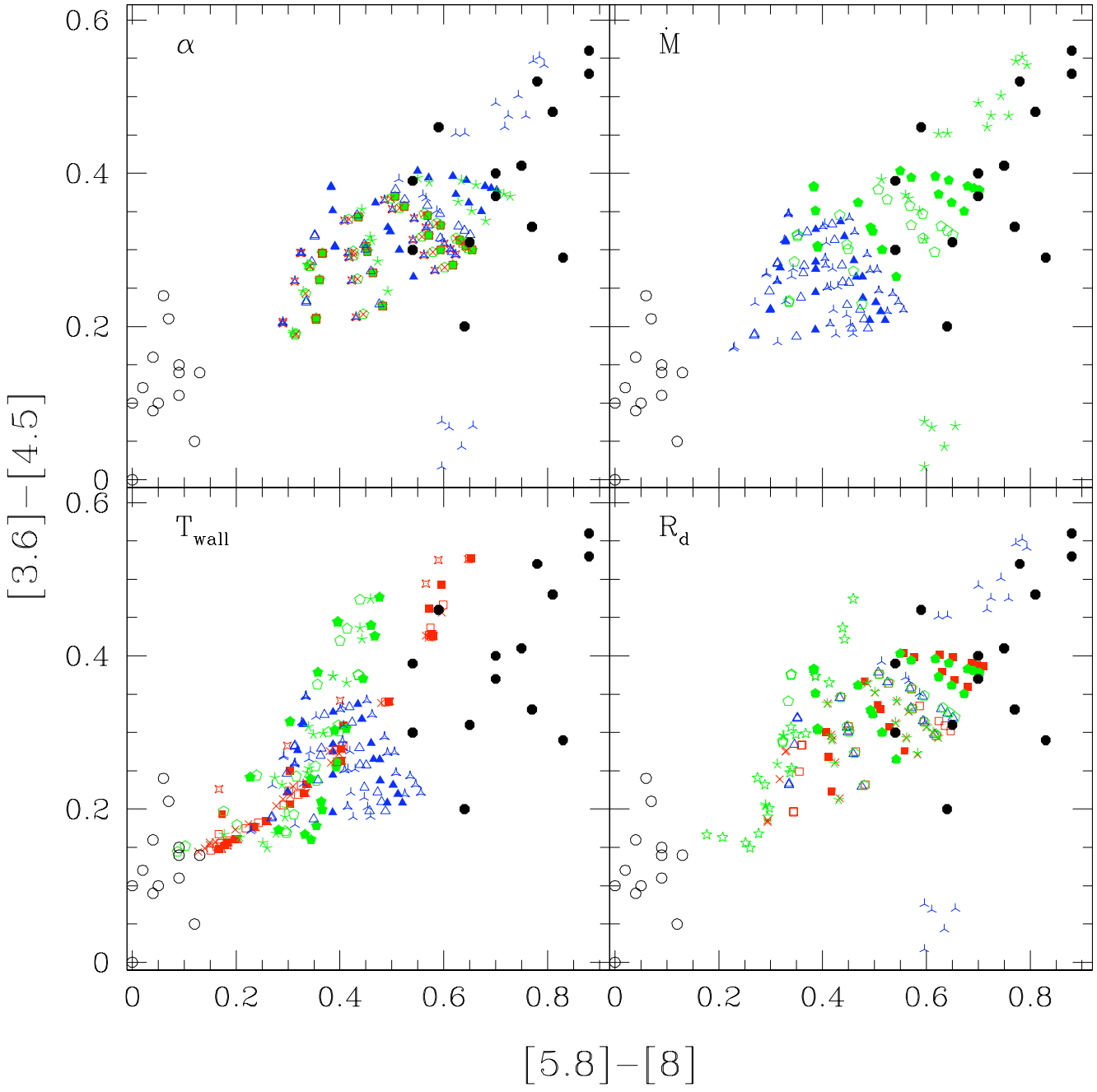

Figure 3: Synthetic color-color plot for the four IRAC bands. Symbols and symbols colors+forms are the same as 2.

D'Alessio, P., Calvet, N., Hartmann, L., Franco-Hernández, R., & Servín, H. 2006, ApJ, 638, 314

Furlan, E., et al. 2006, ApJS, 165, 568

Hartmann, L., Megeath, S. T., Allen, L., Luhman, K., Calvet, N., D'Alessio, P., Franco-Hernandez, R., & Fazio, G. 2005, ApJ, 629, 881

Luhman, K. L. 2004, ApJ, 617, 1216

Luhman, K. L., Whitney, B. A., Meade, M. R., Babler, B. L., Indebetouw, R., Bracker, S., & Churchwell, E. B. 2006, ApJ, 647, 1180

Luhman, K. L., et al. 2007, ApJ, 666, 1219

Fazio, G. G., et al. 2004, ApJS, 154, 10

Guieu, S., et al. 2007, A&A, 465, 855

Rieke, G. H., et al. 2004, ApJS, 154, 25

Scholz, A., Jayawardhana, R., & Wood, K. 2006, ApJ, 645, 1498

Skrutskie, M. F., et al. 2006, AJ, 131, 1163

Werner, M. W., et al. 2004, ApJS, 154, 1